Single-atom substitution enables supramolecular diversity from dipeptide building blocks†

Erica Scarel,[a] Ottavia Bellotto,[a] Petr Rozhin,[a] Slavko Kralj,[bc] Mariagrazia Tortora,[de] Attilio V. Vargiu,[f] Rita De Zorzi,[a] Barbara Rossi*[e] and Silvia Marchesan*[a]

Dipeptides are popular building blocks for supramolecular gels that do not persist in the environment and may find various applications. In this work, we show that a simple substitution on the aromatic side-chain of phenylalanine with either fluorine or iodine enables supramolecular diversity upon self-assembly at neutral pH, leading to hydrogels or crystals. Each building block is characterized by ^{1}H- and ^{13}C-NMR spectroscopy, LC-MS, circular dichroism, and molecular models. The supramolecular behaviour is monitored with a variety of techniques, including circular dichroism, oscillatory rheology, transmission electron microscopy, attenuated total reflectance Fourier-transformed infrared spectroscopy, visible Raman spectroscopy, synchrotron-radiation single-crystal X-ray diffraction and UV Resonance Raman spectroscopy, allowing key differences to be pinpointed amongst the halogenated analogues.

Introduction

Short peptides are attractive, low-cost building blocks for self-assembled materials that do not persist in the environment and can be formed in benign solvents, such as aqueous solutions.[1] Thanks to the great chemical diversity of natural and non-canonical amino acids,[2] it is possible to tune the physico-chemical properties of the final product, and this is an attractive feature for different applications spanning from innovative solutions in medicine[3–6] to energy[7,8] and bioelectronics.[9–11] To enable translation into the market, it is key to design systems with low-cost and easy scale-up. For this reason, the minimal building blocks, *i.e.* dipeptides, are highly attractive,[12] since production costs exponentially increase with amino acid sequence length, with economical liquid-phase synthesis becoming impractical on a large scale for longer sequences.[13]

Prediction of the self-assembly behaviour of dipeptides is remarkably difficult in light of their richness in diverse functional groups and conformational flexibility, so that even subtle structural variations could potentially lead to very divergent outcomes through the cooperative process of self-organization.[14–16] The most popular approach for their design includes the use of polyaromatic N-caps, which facilitate hydrophobically driven self-aggregation and ordered stacking.[14,17] Derivatization can be extended to both termini, introducing non-ionizable groups to reduce the hydrophilic character and, thus, the minimal concentration required for assembly and/or gelation.[18–21] Halogenation is another useful strategy, which has the additional advantage of enabling further non-covalent interactions.[20,22,23] Amino acid chirality is also emerging as a strategy to control dipeptide self-assembly, with heterochirality resulting in increased hydrophobicity, as shown in dipeptides bearing Leu/Ile and Phe amino acids.[24,25]

Diphenylalanine is the most popular dipeptide building block with a remarkable propensity to self-organize into diverse superstructures, such as nanotubes and fibers.[20,26,27] Interestingly, the dipeptide is an unstable gelling agent forming a heterogenous network of fibres of various diameters that shows syneresis, meaning shrinking with concomitant expulsion of the solvent over time.[28] Phenylalanine aromatic rings often participate in aromatic non-covalent interactions that are crucial for self-organisation. Polarization of Phe residues is a strategy to use polar–π interactions between two different aromatic rings as a driving force for assembly. For instance, dipeptides with pentafluorophenylalanine and one aromatic

[a] University of Trieste, Chem. Pharm. Sc. Dept., Via Giorgieri 1, 34127 Trieste, Italy. E-mail: smarchesan@units.it
[b] Jožef Stefan Institute, Materials Synthesis Dept., Jamova 39, 1000 Ljubljana, Slovenia
[c] University of Ljubljana, Pharmaceutical Technology Dept., Faculty of Pharmacy, Aškerčeva 7, 1000 Ljubljana, Slovenia
[d] Area Science Park, Padriciano 99, 34149 Trieste, Italy
[e] Elettra-Sincrotrone Trieste, S.S. 114 km 163.5, Basovizza, 34149 Trieste, Italy. E-mail: barbara.rossi@elettra.eu
[f] University of Cagliari, Physics Dept., 09042 Monserrato, Cagliari, Italy

† Electronic supplementary information (ESI) available: Spectroscopy, rheology, microscopy, photographs, single-crystal XRD, *in silico* and UVRR data. CCDC 2130532 and 2130533. For ESI and crystallographic data in CIF or other electronic format see DOI: 10.1039/d1sm01824h

natural amino acid showed the ability to form gels driven by polar–π interactions.[29] Indeed, Phe halogenation is a strategy to improve the gelling ability of peptides.[20,22,30]

In 2020, our group reported that heterochiral D–Phe–L–Phe surprisingly maintained the ability of homochiral L–Phe–L–Phe to self-assemble into nanotubes through stacking of dipeptides arranged head-to-tail to enclose a hydrophilic inner core.[31] As a result of the different stereoconfiguration, however, only the heterochiral Phe–Phe displayed the two aromatic rings face-to-face, enabling intramolecular interactions at the expense of intermolecular ones. Interestingly, the net result is the stabilization of a double-layer of peptides into 4-nm wide nanotubes, which formed a stable hydrogel, with suppression of the bundling tendency noted for the homochiral Phe–Phe. Monohalogenation of the N-terminal Phe into the corresponding **2-F**, **3-F**, **4-F**, and **4-I** derivatives maintained the ability to gel, with the advantage of a lower minimum gelling concentration (mgc). To extend the toolbox of self-assembling Phe–Phe derivatives, in this work, we show that when this approach is applied to the C-terminus, very different outcomes result from the supramolecular behaviour. Detailed investigation using several techniques, including synchrotron-based UV Resonance Raman (UVRR) spectroscopy, sheds light on key differences in the Phe hydrophobic environment.

Results and discussion

Synthesis and molecular characterization

The four dipeptides shown in Scheme 1 were synthesized by solid-phase reaction, purified by reversed-phase HPLC and analyzed for the purity and identity by LC-MS, ^{1}H-NMR spectroscopy and ^{13}C-NMR spectroscopy (see the ESI,† Sections S1–S5). All dipeptides are heterochiral, and since enantiomers display the same supramolecular behaviour in achiral environments, they are representatives of the four enantiomeric pairs D–L and L–D.

All the fluorinated compounds displayed almost identical retention times (R_t) to their halogenated analogues at the C-terminus.[31] The R_t were all similar, with only **4-I** being slightly more hydrophobic (see the ESI,† Section S5). In diluted solutions, the CD spectra were reminiscent of their analogues halogenated at the N-terminus,[31] with the D–L dipeptides displaying a positive signal above 200 nm, and the two L–D dipeptides displaying a negative signal (Fig. 1A). Previous studies showed that this type of CD signature can be a representative of a population of conformations, which can also be found for non-assembling analogues.[32]

Self-assembly in phosphate buffer

When subjected to a pH trigger from alkaline to neutral (Fig. 2), only **2-F** and **4-F** gelled with mgc values of 15 and 7 mM, respectively. The gels were thermoreversible (see the ESI,† Section S6). Conversely, **3-F** and **4-I** consistently crystallized, allowing for XRD analysis (*vide infra*). Above the mgc, the CD signal rapidly evolved for **2-F** and **4-F** (Fig. 1B). Considering the similar HPLC retention times (see the ESI,† Section S5), molecular hydrophobicity is not a discriminating parameter for gelation within this series.

The amide I and III regions of the FT-IR spectra were dominated in all cases by signals at 1680, 1210 and 1255 cm^{-1}, with an additional peak at 1228 cm^{-1} for **2-F**, which were all compatible with β-sheet-like hydrogen-bonding networks.[33] Other signals in the amide I region included a peak at

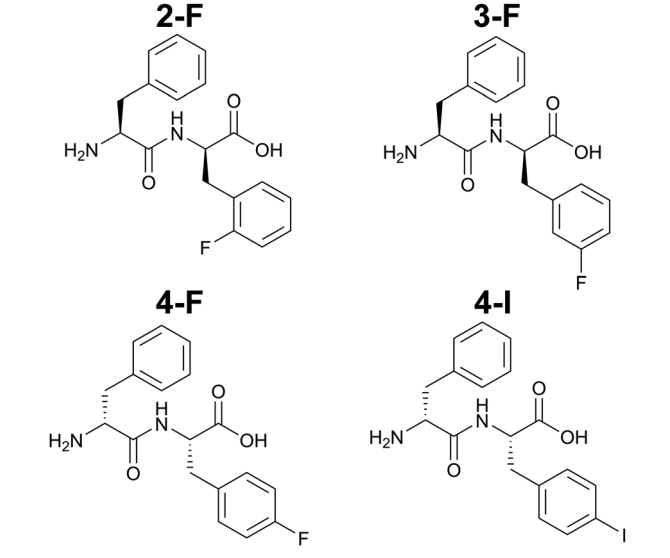

Scheme 1 Chemical structures of the four heterochiral Phe–Phe dipeptides.

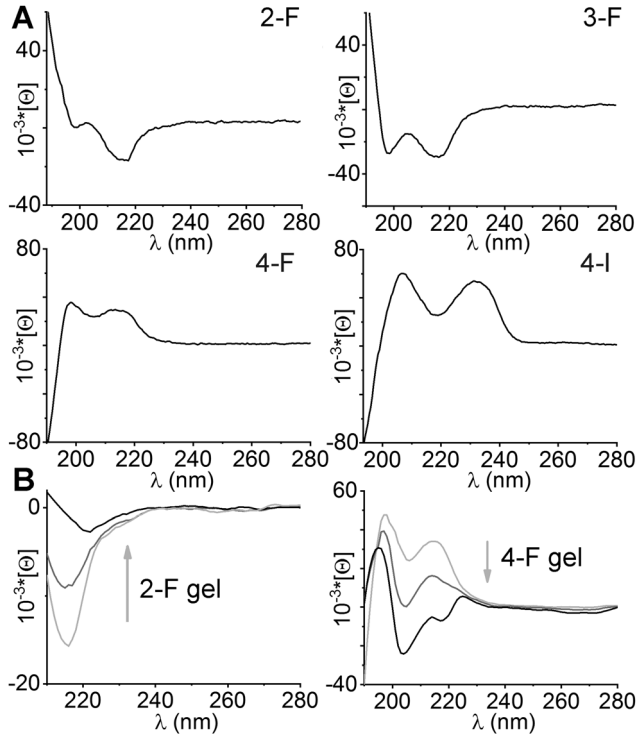

Fig. 1 CD spectra of the dipeptides in solution (A) and in the gel state (B). The grey arrow indicates signal evolution over time.

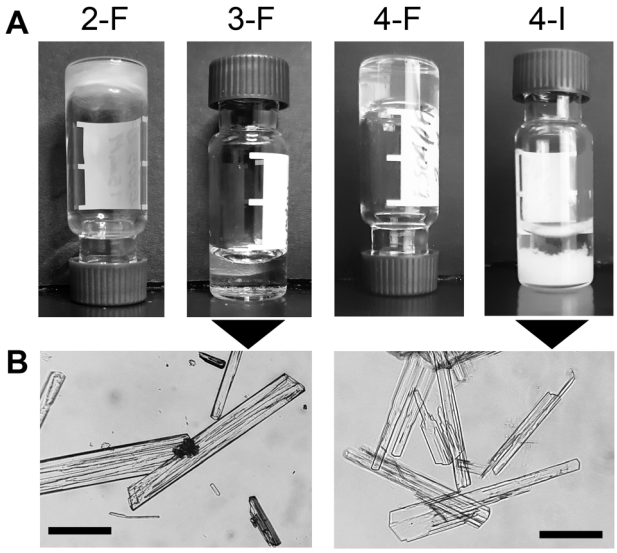

Fig. 2 (A) Photographs of the four compounds in phosphate buffer (pH 7.3) above their solubility limit. (B) Optical microscopy image (10×) of the crystals formed by the **3-F** (left) and **4-I** (right) dipeptides. Scale bar = 200 μm.

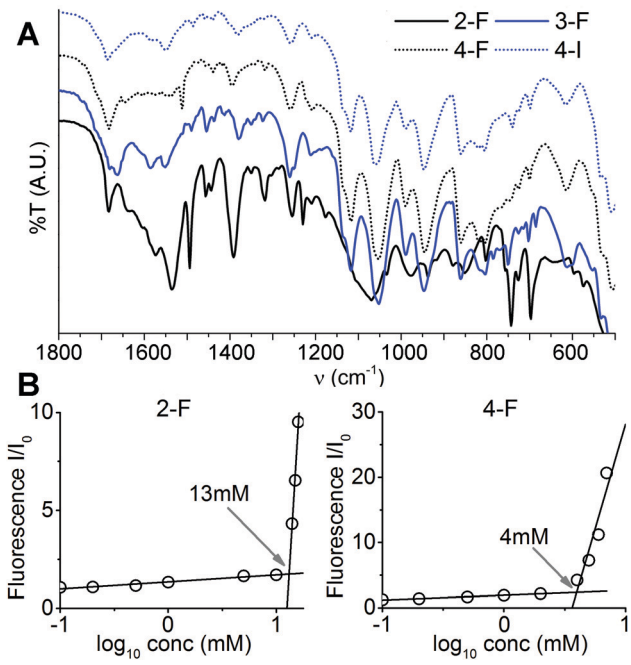

Fig. 3 (A) ATR FT-IR spectra of the four dipeptides upon application of the pH trigger. (B) Thioflavin T fluorescence for the two gelators allowed the corresponding critical aggregation concentration to be calculated (cac, see the grey arrow).

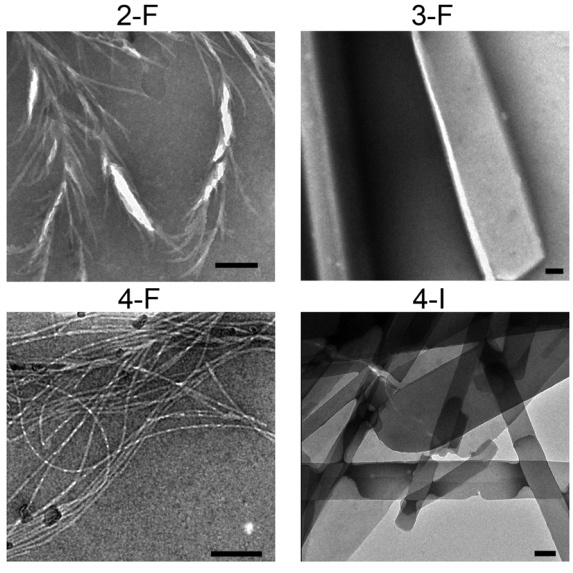

Fig. 4 Transmission electron microscopy (TEM) images of the four dipeptides under self-assembly conditions. Scale bar = 200 μm.

1639 cm^{-1}, compatible with β-sheet-like stacks, for the two gelators **2-F** and **4-F**, which was not evident in the case of **3-F** and **4-I** analogues. The amide II band, which is of more difficult interpretation, was also similar for the two gelators (1534 and 1572 cm^{-1}), and with blue-shifted signals for the other two compounds (1551 and 1585 cm^{-1}), in agreement with the more extended H-bonding network for the latter. The signal at 1570 cm^{-1} was already reported for fibrillating dipeptides, and it had been attributed to the strong association between the charged N- and C-termini in the supramolecular state.[24,34]

The formation of β-sheet-like stacks was confirmed by thioflavin T fluorescence for the two gelators that formed homogeneous systems, enabling quantitative analysis. In both cases, amyloid-associated fluorescence allowed the corresponding critical aggregation concentration (cac)[35] to be estimated as 13 and 4 mM for **2-F** and **4-F**, respectively (Fig. 3B). Transmission electron microscopy (TEM) confirmed the presence of microcrystals for **3-F** and **4-I** and of fibrils for the gelling **2-F** and **4-F** (Fig. 4 and ESI,† Section S7). In particular, the fibrils of the **2-F** dipeptide displayed an average diameter of 17.5 ± 5.8 nm (n = 200) but also a marked tendency to bundle into fibres as thick as 100 nm, with many instances of fibres branching into fibrils and interconnecting points between the latter. This type of nanostructure is in agreement with the opaque appearance of the corresponding hydrogel and denotes a marked difference in the supramolecular behaviour relative to D–Phe–L–Phe that does not bundle.[31] Conversely, the **4-F** dipeptide formed a highly homogenous population of fibrils with an average diameter of 11.9 ± 1.8 nm (n = 100) that could run parallel for some lengths but without fusing into fibres, which was in agreement with the translucent appearance of the hydrogel. Previous studies on protein complexes suggested that fluorination in the *ortho* position can lead to stronger intermolecular stacking interactions, relative to the *para* position, and they could take part in fibril bundling observed only for **2-F**, but not **4-F**.[36] Local and direct positive effects of electron-withdrawing substitutions on aromatic stacking interactions are established.[37]

Oscillatory rheology confirmed the gel nature of the **2-F** and **4-F** compounds, whose gelation reached a plateau within 15 minutes, with elastic modulus G' values of 18 kPa and

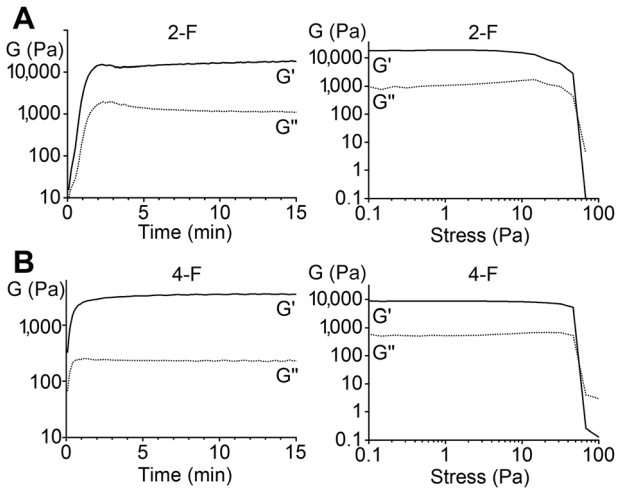

Fig. 5 Oscillatory rheology time sweeps (left) and stress sweeps (right) for the two gelators **2-F** (A) and **4-F** (B) at their mgc.

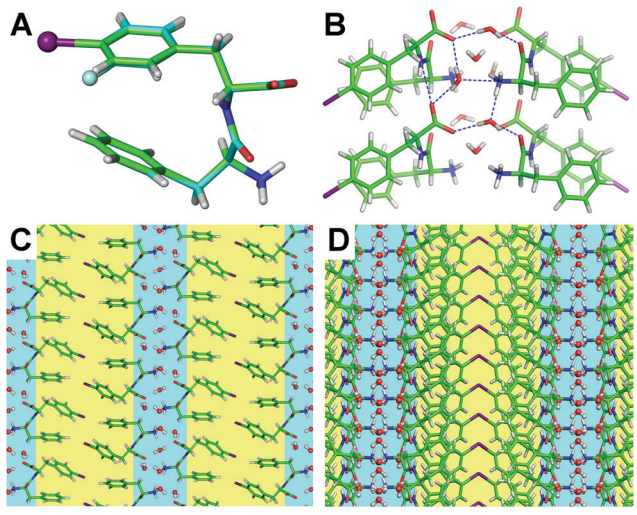

Fig. 6 Single-crystal XRD data. (A) Superimposition of D–Phe–L–(**3-F**)–Phe (CCDC 2130532, carbon atoms in cyan) and D–Phe–L–(**4-I**)–Phe (carbon atoms in green). (B) Hydrophilic interactions of **4-I** (CCDC 2130533). (C and D) Supramolecular packing of **4-I** into hydrophobic (yellow) and hydrophilic (cyan) regions. (C) Top-view and (D) side-view of the peptide stacks.

8 kPa, respectively, at their corresponding mgc (Fig. 5 and ESI,† Section S8). Unsurprisingly, the gelation kinetics for **2-F** were slower than for **4-F**, as only the fibrils of the former bundled during the process, as confirmed by TEM (Fig. 4). Similarly, the decrease in viscoelastic moduli accompanying the gel-to-sol transition in the stress sweeps (Fig. 5) was wider for the former, whose gel is composed of a heterogeneous population of fibrils and fibers.

Single-crystal X-ray diffraction (XRD)

The two compounds **3-F** and **4-I** consistently crystallized when subjected to the pH trigger (Fig. 1), thus allowing for their study by X-ray diffraction (XRD, Fig. 6). In both cases, the asymmetric unit contains a molecule of the peptide in its zwitterionic form and three molecules of water (see the ESI,† Section S9).

Despite the notable differences between the iodine and fluorine radii, there is a striking similarity between the two structures, as evident from the superimposition of the peptide backbones of D–Phe–L–(**3-F**)–Phe and D–Phe–L–(**4-I**)–Phe, that adopt the same conformation (Fig. 6A). Furthermore, both peptides interact in the same way with their polar groups within the hydrophilic layer, although minor differences are noted in the hydrophobic layer where the halogen atoms reside (see the ESI,† Section S9). In both cases, crystal packing shows a separation between the hydrophobic layers (shown in yellow in Fig. 6C and D) with the prevalence of phenyl groups and hydrophilic layers (shown in cyan in Fig. 6C and D) with the peptide backbones and water molecules. In particular, in hydrophilic layers, peptides form piles in the crystallographic direction *b*, held together by hydrophilic interactions, most of which are mediated by solvent molecules (Fig. 6B), which is a recurring feature of fibrillating dipeptides that do not gel.[24,25] The iodine atoms are equally spaced along the *a* crystallographic direction, with an average distance of 4.6 Å and no evidence of halogen bonding. This type of packing for **4-I** is not too surprising since a similar situation was found for the analog D–(**4-I**)–Phe–L–Phe.[31] Conversely, the fact that **3-F** shows the same type of layered packing is unexpected, since all the analogues that were fluorinated at the N-terminus formed, instead, supramolecular water channels.[31]

Molecular models of the four dipeptides did not reveal clear-cut trends in the orientation or magnitude of the dipole moment that could explain the higher propensity towards the crystallization of **3-F** and **4-I**, relative to **2-F** and **4-F** (see the ESI,† Section S10). This finding is in agreement with previous studies on fluorination at different positions of benzene and its effects on intermolecular interactions involved in protein complexes.[36] Other studies have also shown that electron-density dispersion has a major contribution relative to electrostatics, in stabilizing stacking interactions between aromatic rings, of which one is fluorinated.[38] However, the minimized conformations of gelling **2-F** and **4-F** were very different relative to those found in the crystal structures of the former two. In particular, the dipeptide molecules were more extended with the phenyl rings further apart in a position that appears to be unfavourable for the establishment of intramolecular interactions (Fig. 7 and ESI,† Section S10) and the exclusion of water from hydrophobic layers as seen in Fig. 6C and D. The gels were tested for powder XRD, but no diffraction was observed. Thus, Raman spectroscopy was used to shed further light on the packing of the four compounds.

Visible Raman spectroscopy

Recently, we applied Raman spectroscopy to analyse the self-assembling behavior of short peptides based on the Phe–Phe motif.[39] In particular, this technique proved useful to assess the presence of halogen bonding and identify differences due to the supramolecular packing, in the crystal and gel phases, compared with the powder form.[31]

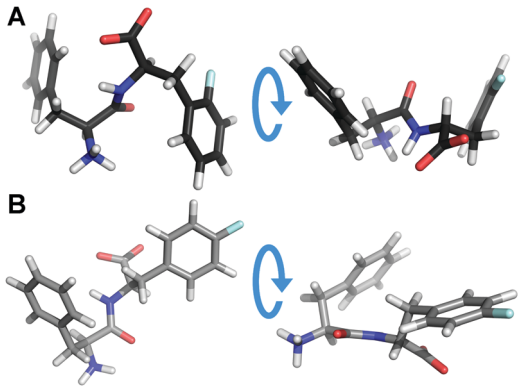

Fig. 7 Energy-minimized molecular models for **2-F** (A) and **4-F** (B) gelators.

Visible Raman spectra of the dipeptides in their powder form and gel or crystal states are shown in Fig. 8. Due to the Raman interfering signal of water in the spectral region of interest, spectra were collected on dry samples. The most intense Raman signals are assigned to Phe, hereafter referred to as F1 ($\approx$1004 cm^{-1}) and F2 ($\approx$1034 cm^{-1}). Both these modes are due to side-chain vibrational motions of the Phe ring; in particular, the F1 band is due to the benzene breathing mode, while the F2 signal is associated with the in-plane CH bending.[40,41] Interestingly, the F2 band displays a blue shift of 4–5 cm^{-1} only for **3-F** and **4-I** in the crystals (insets in Fig. 8B and D). Conversely, no significant spectral changes for F1 and F2 were detected upon assembly of **2-F** and **4-F** into gels. This distinct behaviour may be related to the different packing of the Phe rings in the crystal or gel state, in agreement with molecular models. Furthermore, new signals (denoted with * in Fig. 8) arose with assembly in all cases, of which those at 1256 cm^{-1} and 1687 cm^{-1} were evident only for **2-F** and **4-F** gels, respectively. These peaks were attributed to the amide III and amide I bands related to the formation of extended H-bond networks in β-sheet-like stacks of dipeptide gels.[25] However, in this region, both aromatic and amide signals overlapped, and for this reason, UVRR spectroscopy was needed (*vide infra*). Finally, no shifts due to halogen bonding were noted,[31] in agreement with XRD.

UV Resonance Raman (UVRR) spectroscopy

Thanks to the resonance effect, UV Resonance Raman (UVRR) spectroscopy offers several advantages with respect to the conventional visible Raman technique, such as the significant increment of the detection limit and the selectivity needed to incisively monitor specific chromophores within the sample. The fine tunability of the synchrotron radiation source allows an accurate choosing of UVRR excitation wavelengths to efficiently disentangle the Raman bands associated with specific chemical groups. These conditions determine the usefulness of UVRR spectroscopy as a highly sensitive and selective spectral probe for exploring peptides under very diluted or concentrated conditions in water. UVRR spectra of peptides usually contain many vibrational fingerprints that can be related to the conformation and intermolecular interactions. In particular, the excitation wavelength at 226 nm is the most suitable for investigating the aromatic signals of Phe due to the close resonance of this excitation energy with their electronic transitions.[42,43] This results in a strong enhancement of the UV Raman cross-section of some vibrational modes of Phe whose Raman signal dominates the UVRR spectrum, as confirmed by analysis of amino acid precursors devoid of the amide bond (see the ESI,† Section S11). The prominent Raman band observed between 1580 and 1620 cm^{-1} in the spectra of Fig. 9 is attributable to the in-plane ring stretching mode ν_{8a} of Phe[44] and is very sensitive to ring substituents.[45] In unsubstituted Phe, it appears at 1609 cm^{-1},[44,45] while *p*-substitution in **4-F** and **4-I** causes red shifts to 1604 and 1584 cm^{-1}, respectively. Conversely, a red shift to 1614 cm^{-1} is found for **2-F** and **3-F** (Fig. 9 and ESI,† Section S11).

Phe can be involved in hydrophobic, cation–π and H-bond interactions with nearby residues or surrounding molecules of

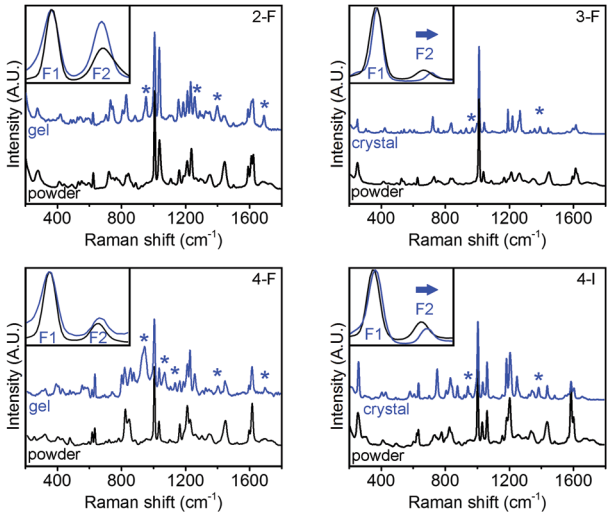

Fig. 8 Visible Raman spectra of the four dipeptides.

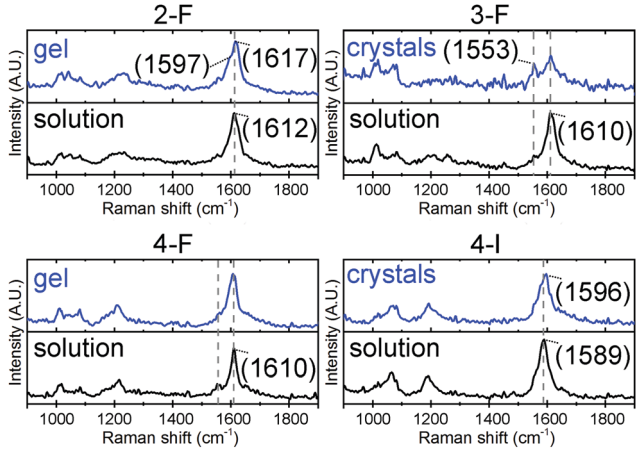

Fig. 9 UVRR spectra of the four dipeptides in their precursor solutions (black traces) and after the pH trigger to neutral (blue traces) that yielded hydrogels (**2-F** and **4-F**) or crystal suspensions (**3-F** and **4-I**).

a solvent.[46] Both the wavenumber position and intensity of the Raman band assigned to the ring-stretching mode ν_{8a} were reported to be very sensitive to the local environment in peptide self-assembly.[47] In the case of **2-F**, the Raman signal corresponding to the ring-stretching mode of Phe is detected at $\sim$1612 cm^{-1} in solution (Fig. 9). Gelation causes a 5 cm^{-1} red shift to 1617 cm^{-1} and the appearance of a shoulder at 1597 cm^{-1}. The blue shift is indicative of aromatic interactions arising from fibrillisation, whilst splitting of the Raman signal could arise from interlayer interactions on the stacking order in the **2-F** gel, which is formed by fibrils and fibres of various diameters.

In the case of **4-F**, only a broadening of the ν_{8a} signal at 1610 cm^{-1} occurred upon assembly. The Raman cross section of these bands has been demonstrated to markedly depend on the exposure to water of the aromatic ring.[48] This finding could suggest a minor strength of the stacking interactions among Phe rings in **4-F** hydrogels, which indeed arise from fibrils that do not further bundle into fibers, and are thus more exposed to the solvent relative to the **2-F** hydrogel. UVRR is thus consistent with TEM.

Crystals of **3-F** and **4-I** were more difficult to analyze due to the heterogeneity of their dispersions in the liquid buffer. Indeed, the UVRR signal is collected from a spot size of several mm^2; thus, homogeneous gels of **2-F** and **4-F** allow for higher quality data relative to crystal dispersions of **3-F** and **4-I**. In the case of **4-I**, after several measurements, good-quality spectra were obtained that allowed a 7 cm^{-1} blue shift arising from the hydrophobic interactions of the Phe rings to be discerned, which was in agreement with the XRD data (see Fig. 6). Unfortunately, in the case of **3-F**, the partial loss of the UV-resonant aromatic signals was noted, with the appearance of the non-resonant amide II signal at 1553 cm^{-1}, and no Phe-associated shifts could be unambiguously seen. However, since **3-F** and **4-I** display analogous packing, superimposable peptide backbones, and positions of water molecules (Fig. 6 and ESI† Section S9), we expect a similar situation to **4-I**.

Overall, UVRR allowed the amide and Phe aromatic signals to be disentangled and the inherent shifts due to halogen-substitution to be unambiguously assigned. Secondly, UVRR enabled the monitoring of variations in the Phe environment arising from the assembly of the different peptides.

Experimental

Materials and methods

Fmoc-amino acids, 2-chlorotrityl chloride resin, and coupling agents were obtained from GL Biochem (Shanghai) Ltd. All other chemicals and solvents were acquired at analytical grade from Merck. An in-line Millipore RiOs/Origin system provided high-purity Milli-Q-water with a resistivity $>$18 M Ω cm. ^{1}H-NMR and ^{13}C-NMR spectra were recorded using a Varian Innova spectrometer at 400 MHz with chemical shifts reported as ppm (using tetramethylsilane as the internal standard). An Agilent 6120 LC-MS system was used for ESI-MS spectra. Optical microscopy images were acquired on a drop of fresh samples deposited on clean glass slides, using a Leitz Labovert instrument with a 10× magnification objective.

Synthetic procedures

Each dipeptide was synthesized by solid phase synthesis using a standard Fmoc-protection strategy as previously described.[39] Purification was performed using an Agilent 1260 chromatography system using a C-18 column (Kinetex, 5 μm, 100 Å, 250 × 10 mm, Phenomenex) and acetonitrile (MeCN) and water with 0.05% TFA as an eluent mixture with the following methods. For **2-F**, **3-F**, **4-F**: t = 0 min. 30% MeCN, t = 2 min. 30% MeCN, t = 12 min. 55% MeCN, t = 15 min. 95% MeCN. For **4-I**: t = 0 min. 30% MeCN, t = 2 min. 30% MeCN, t = 12 min. 42% MeCN, t = 15 min. 95% MeCN. Fractions with the products were freeze-dried.

Self-assembly into hydrogels or crystals

Each peptide was dissolved in sodium phosphate buffer (0.1 M, pH 11.8). An equal volume of acidic sodium phosphate buffer (0.1 M, pH 5.8) was added to reach the final concentration.

ATR-IR and visible Raman spectroscopy

Samples were prepared at their mgc for the two gelators (7 mM for **4-F** and 15 mM for **2-F**) or above their solubility limit for **3-F** (10 mM) and **4-I** (4 mM) and left to dry under vacuum overnight using a 1 cm^2 piece of silicon wafer for ATR or on a glass slide for Raman. ATR-IR spectra were acquired using an IRAffinity-1S spectrophotometer (Shimadzu) at 4 cm^{-1} resolution and 240 scans. Raman spectra were acquired using a 532 nm laser (5–10% power) with a Renishaw instrument.[39] Spectra were recorded with 10–20 accumulations in several spots per sample, with a 1 cm^{-1} resolution.

Circular dichroism

Peptides were dissolved at the desired concentration (1 mM for **2-F**, **3-F** and **4-F**; 0.1 mM for **4-I**) using the method described above. Samples were placed in a 0.1 mm quartz cuvette on a Jasco J-815 spectropolarimeter at 25 °C (Peltier), with a 1 nm resolution. 5–10 spectra were averaged to reduce noise. CD spectra were also acquired at higher concentrations to monitor evolution upon assembly. In particular, for **2-F** (5 mM) and **4-F** (14 mM), the corresponding spectra during the first 15 minutes (averaged every 5 minutes) are shown in Fig. 1B.

Crystallography

Single crystals of **3-F** (CCDC 2130532) and **4-I** (CCDC 2130533) were obtained upon assembly as described above. For each compound, a single crystal was collected using a loop, cryoprotected by dipping it in glycerol, and then frozen in liquid nitrogen for storage. The crystal was mounted on the diffractometer at the synchrotron Elettra, Trieste (Italy), XRD1 beamline, using the robot available at the facility. The temperature was set at 100 K. Diffraction data were collected by rotating the crystal, using synchrotron radiation with a wavelength of 0.70 Å. Further details on the structure determination and parameters

of the cell unit are in the ESI.† Deposition numbers 2130532 and 2130533 refer to the crystallographic data deposited at the Cambridge Crystallographic Data Centre (CCDC).

Molecular models

Molecular models of the four dipeptides in implicit water were generated using quantum-level calculations to assess intrinsic preferences towards compact or extended conformations of the single component of the assembly and to estimate the values of molecular dipoles. See the ESI† (Section S10) for more details.

Oscillatory rheology

Hydrogels were prepared *in situ* using a Kinexus Plus rheometer (Malvern) with a stainless steel parallel plate geometry. Each experiment was performed with a 1 mm gap at 25 °C (Peltier). Time sweeps were measured at 1 Pa and 1 Hz, frequency sweeps were measured at 1 Pa and stress sweeps were measured at 1 Hz. Each sample was analysed at least three times and representative measurements are shown.

TEM analysis

Samples were prepared as described above at their mgc for **2-F** and **4-F** and at 10 mM (**3-F**) or 4 mM (**4-I**). They were transferred onto TEM carbon grids previously exposed to a UV-Ozone Procleaner Plus for 5 min. A drop of aqueous tungstate phosphate solution (pH 7.2) was added as the contrast agent and all the samples were dried *in vacuo*. TEM images were acquired using a Jeol JEM 2100 microscope (Japan) at 100 kV and analysed using the FIJI free software.

Thioflavin T fluorescence

Spectra were recorded using an Infinite M1000 pro microplate reader (TECAN) with Greiner 96 U bottom black polystyrene plates (VWR). Samples of **2-F** and **4-F** were prepared as described above at a desired final concentration (120 μL) and, after 1 hour of assembly, 30 μL of thioflavin solution was added (23.5 μM in 20 mM glycine–NaOH pH 7.4). After 15 minutes, fluorescence was analysed with λ_{ex} 446 nm and λ_{em} 490 nm (20 nm bandwidth). Experiments were run twice in triplicate (n = 6).

UV Resonance Raman spectroscopy

UVRR spectra were acquired using excitation radiation at 226 nm by exploiting the synchrotron-based UVRR set-up available at the BL10.2-IUVS beamline of Elettra Synchrotron Trieste (Italy). The energy of the excitation wavelength was set by regulating the undulator gap and using a Czerny–Turner monochromator (Acton SP2750, Princeton Instruments, Acton, MA, USA) equipped with a holographic grating with 3600 groves mm^{-1} for monochromatizing the incoming synchrotron radiation. All the UVRR spectra were collected in back-scattered geometry by using a single pass of a Czerny–Turner spectrometer (Trivista 557, Princeton Instruments, 750 mm of focal length) equipped with a holographic grating at 1800 g mm^{-1}. The spectral resolution was set at 2 cm^{-1} $pixel^{-1}$. The calibration of the spectrometer was standardized using cyclohexane (spectroscopic grade, Sigma Aldrich). Any possible photo-damage effects due to prolonged exposure of the sample to UV radiation (the maximum beam power measured on the sample was tens of μW) was avoided by continuously spinning the sample cell during measurements. All the samples were freshly dissolved in buffer for assembly and placed in quartz cuvettes for UVRR measurements. The temperature was set at 298 K.

Conclusions

In this work, we report on the differing effects of Phe halogenation at the C-terminus, as opposed to the N-terminus, of heterochiral Phe–Phe, which provides gelators in all cases.[31] In particular, the peptides **3-F** and **4-I** demonstrate a strong propensity towards crystallization, with analogous supramolecular packing into amphipathic layers, and the absence of iodine-mediated halogen bonding. Conversely, **2-F** and **4-F** self-assemble into thermoreversible hydrogels, albeit with differing amyloid nanostructures, cac, mgc, and viscoelastic properties. Remarkably, the presence of fluorine in the *para*-position at the C-terminus maintained the suppression of hierarchical bundling noted for heterochiral Phe–Phe,[31] whilst the opposite was true for the *ortho* position. Molecular models and visible and UV Resonance Raman spectroscopy indicate that the diverging behaviour is not due to molecular dipoles, but to the tendency of the Phe rings to adopt differing spatial orientations, which ultimately affect the peptides' ability to establish more or less hydrophobic regions that exclude water and stabilize gelling fibrils. In the future, it would be interesting to expand the application of UVRR to monitor diagnostic amyloid signals to other assembling peptides in an attempt to better identify more general rules for their self-assembly in physiologically relevant conditions.

Author contributions

Investigation: E. S., O. B., P. R., S. K., M. T., A. V. V., and R. D. Z. Supervision: A. V. V., R. D. Z., B. R., and S. M. Writing – initial draft: E. S. Analysis, writing – review and editing: all authors. Conceptualization and methodology: B. R. and S. M.

Conflicts of interest

There are no conflicts to declare.

Acknowledgements

The authors acknowledge Elettra Sincrotrone Trieste for providing access to its synchrotron radiation facilities, M. Polentarutti and G. Bais for assistance with beamline XRD1, A. Gessini for assistance on IUVS beamline, the CENN Nanocenter (Slovenia) for access to TEM, and the Slovenian Research Agency (RSA – ARRS) through the core funding No. P2-0089 and ARRS projects No. J2-3043, J2-3040, J2-3046, and J3-3079. M. T. thanks the European Regional Development Fund, Interreg V-A Italy

Austria 2014–2020, project ITAT 1059 InCIMa4 ''InCIMa for Science and SMEs''.

References

1 A. Lampel, *Chem*, 2020, **6**, 1222–1236.
2 R. Misra, S. Rudnick-Glick and L. Adler-Abramovich, *Macromol. Biosci.*, 2021, **21**, 2100090.
3 T. Hu, O. Agazani, S. Nir, M. Cohen, S. Pan and M. Reches, *ACS Appl. Mater. Interfaces*, 2021, **13**, 48469–48477.
4 M. Kurbasic, E. Parisi, A. M. Garcia and S. Marchesan, *Curr. Top. Med. Chem.*, 2020, **20**, 1300–1309.
5 E. R. Cross, S. M. Coulter, S. Pentlavalli and G. Laverty, *Soft Matter*, 2021, **17**, 8001–8021.
6 P. Singh, N. Wangoo and R. K. Sharma, *Soft Matter*, 2020, **16**, 4105–4109.
7 K. Tao, B. Xue, S. Han, R. Aizen, L. J. W. Shimon, Z. Xu, Y. Cao, D. Mei, W. Wang and E. Gazit, *ACS Appl. Mater. Interfaces*, 2020, **12**, 45192–45201.
8 E. Nikoloudakis, M. Pigiaki, M. N. Polychronaki, A. Margaritopoulou, G. Charalambidis, E. Serpetzoglou, A. Mitraki, P. A. Loukakos and A. G. Coutsolelos, *ACS Sustainable Chem. Eng.*, 2021, **9**, 7781–7791.
9 R. Garifullin and M. O. Guler, *Mater. Today Bio*, 2021, **10**, 100099.
10 S. J. Percival, S. Russo, C. Priest, R. C. Hill, J. A. Ohlhausen, L. J. Small, S. B. Rempe and E. D. Spoerke, *Soft Matter*, 2021, **17**, 6315–6325.
11 K. Gayen, S. Hazra, A. K. Pal, S. Paul, A. Datta and A. Banerjee, *Soft Matter*, 2021, **17**, 7168–7176.
12 E. R. Draper and D. J. Adams, *Langmuir*, 2019, **35**, 6506–6521.
13 D. J. Adams, *Macromol. Biosci.*, 2011, **11**, 160–173.
14 C. Gila-Vilchez, M. C. Manas-Torres, J. A. Gonzalez-Vera, F. Franco-Montalban, J. A. Tamayo, F. Conejero-Lara, J. M. Cuerva, M. T. Lopez-Lopez, A. Orte and L. Alvarez de Cienfuegos, *Polym. Chem.*, 2021, **12**, 6832–6845.
15 M. C. Manas-Torres, C. Gila-Vilchez, J. A. Gonzalez-Vera, F. Conejero-Lara, V. Blanco, J. M. Cuerva, M. T. Lopez-Lopez, A. Orte and L. Alvarez de Cienfuegos, *Mater. Chem. Front.*, 2021, **5**, 5452–5462.
16 N. A. Dudukovic, B. C. Hudson, A. K. Paravastu and C. F. Zukoski, *Nanoscale*, 2018, **10**, 1508–1516.
17 D. Giuri, L. J. Marshall, C. Wilson, A. Seddon and D. J. Adams, *Soft Matter*, 2021, **17**, 7221–7226.
18 A. M. Gil, J. Casanovas, E. Mayans, A. I. Jimenez, J. Puiggali and C. Aleman, *J. Phys. Chem. B*, 2020, **124**, 5913–5918.
19 E. Nikoloudakis, K. Mitropoulou, G. Landrou, G. Charalambidis, V. Nikolaou, A. Mitraki and A. G. Coutsolelos, *Chem. Commun.*, 2019, **55**, 14103–14106.
20 S. Maity, P. Das and M. Reches, *Sci. Rep.*, 2015, **5**, 16365.
21 S. Maity, S. Nir and M. Reches, *J. Mater. Chem. B*, 2014, **2**, 2583–2591.
22 P. Ravarino, D. Giuri, D. Faccio and C. Tomasini, *Gels*, 2021, **7**, 43.
23 A. Pizzi, L. Catalano, N. Demitri, V. Dichiarante, G. Terraneo and P. Metrangolo, *Pept. Sci.*, 2020, **112**, e24127.
24 O. Bellotto, S. Kralj, M. Melchionna, P. Pengo, M. Kisovec, M. Podobnik, R. De Zorzi and S. Marchesan, *ChemBioChem*, 2022, **23**, e202100518.
25 O. Bellotto, S. Kralj, R. De Zorzi, S. Geremia and S. Marchesan, *Soft Matter*, 2020, **16**, 10151–10157.
26 J. Xia, B. Sun, C. Wang, N. Sun, H. Cao, Y. Jia, Y. Yang and J. Li, *J. Colloid Interface Sci.*, 2021, **599**, 661–666.
27 X. Li, Q. Li, J. Fei, Y. Jia, H. Xue, J. Zhao and J. Li, *Angew. Chem., Int. Ed.*, 2020, **59**, 11932–11936.
28 M. P. Conte, N. Singh, I. R. Sasselli, B. Escuder and R. V. Ulijn, *Chem. Commun.*, 2016, **52**, 13889–13892.
29 H. Zhang, S. Lou and Z. Yu, *Langmuir*, 2019, **35**, 4710–4717.
30 C. Wu, Z. Zheng, Y. Guo, C. Tian, Q. Xue and G. Liang, *Nanoscale*, 2017, **9**, 11429–11433.
31 S. Kralj, O. Bellotto, E. Parisi, A. M. Garcia, D. Iglesias, S. Semeraro, C. Deganutti, P. D'Andrea, A. V. Vargiu, S. Geremia, R. De Zorzi and S. Marchesan, *ACS Nano*, 2020, **14**, 16951–16961.
32 A. M. Garcia, D. Iglesias, E. Parisi, K. E. Styan, L. J. Waddington, C. Deganutti, R. De Zorzi, M. Grassi, M. Melchionna, A. V. Vargiu and S. Marchesan, *Chem*, 2018, **4**, 1862–1876.
33 B. R. Singh, in *Infrared Analysis of Peptides and Proteins*, American Chemical Society, 1999, vol. 750, ch. 1, pp. 2–37.
34 N. S. de Groot, T. Parella, F. X. Aviles, J. Vendrell and S. Ventura, *Biophys. J.*, 2007, **92**, 1732–1741.
35 V. Castelletto, P. Ryumin, R. Cramer, I. W. Hamley, M. Taylor, D. Allsop, M. Reza, J. Ruokolainen, T. Arnold, D. Hermida-Merino, C. I. Garcia, M. C. Leal and E. Castaño, *Sci. Rep.*, 2017, **7**, 43637.
36 Y. Benitex and A. M. Baranger, *J. Am. Chem. Soc.*, 2011, **133**, 3687–3689.
37 S. E. Wheeler, *J. Am. Chem. Soc.*, 2011, **133**, 10262–10274.
38 M. O. Sinnokrot and C. D. Sherrill, *J. Am. Chem. Soc.*, 2004, **126**, 7690–7697.
39 D. Iglesias, M. Melle-Franco, M. Kurbasic, M. Melchionna, M. Abrami, M. Grassi, M. Prato and S. Marchesan, *ACS Nano*, 2018, **12**, 5530–5538.
40 B. Hernández, F. Pflüger, S. G. Kruglik and M. Ghomi, *J. Raman Spectrosc.*, 2013, **44**, 827–833.
41 W. B. Fischer and H. H. Eysel, *Spectrochim. Acta, Part A*, 1992, **48**, 725–732.
42 S. A. Oladepo, K. Xiong, Z. Hong, S. A. Asher, J. Handen and I. K. Lednev, *Chem. Rev.*, 2012, **112**, 2604–2628.
43 Z. Chi and S. A. Asher, *Biochemistry*, 1998, **37**, 2865–2872.
44 S. A. Asher, M. Ludwig and C. R. Johnson, *J. Am. Chem. Soc.*, 1986, **108**, 3186–3197.
45 S. P. A. Fodor, R. A. Copeland, C. A. Grygon and T. G. Spiro, *J. Am. Chem. Soc.*, 1989, **111**, 5509–5518.
46 H. Takeuchi, *Anal. Sci.*, 2011, **27**, 1077–1086.
47 A. A. Profit, V. Felsen, J. Chinwong, E. R. Mojica and R. Z. Desamero, *Proteins*, 2013, **81**, 690–703.
48 N. Kuhar, S. Sil and S. Umapathy, *Spectrochim. Acta, Part A*, 2021, **258**, 119712.